Pediatric Radiology (2021) 51:1826–1838
https://doi.org/10.1007/s00247-021-05064-1

ORIGINAL ARTICLE

Brain fetal magnetic resonance imaging to evaluate maturation of normal white matter during the third trimester of pregnancy

Camille Letissier[1] · Amandine Crombé[2,3] · Lydie Chérier[1] · Jean Delmas[1] · Jean-François Chateil[1,4]

Received: 23 July 2020 / Revised: 2 December 2020 / Accepted: 17 March 2021 / Published online: 21 May 2021

Abstract

Background Quantitative magnetic resonance imaging (MRI) could improve the estimation of fetal brain maturation and the interpretation of white matter signal intensity in pathological conditions.

Objective To investigate T2-based and diffusion-weighted imaging (DWI) measurements for the evaluation of fetal brain maturation during the last trimester of pregnancy.

Materials and methods One hundred sixty-eight fetal brain MRIs were retrospectively analyzed (age range: 28–37 weeks of gestation) after ensuring that none of the children developed psychomotor or cognitive impairment (median follow-up: 4.7 years). Bilateral regions of interest were drawn on the frontal, occipital, parietal and temporal lobes from T2-W imaging and DWI, when available, to evaluate signal intensity and apparent diffusion coefficient (ADC) values. Ratios were calculated with two references (pons or thalamus and cerebrospinal fluid) to standardize signal intensities. Reproducibility was evaluated with intraclass correlation coefficients (ICCs) and Bland-Altman plots. Correlations with gestational age were evaluated with univariate and multivariate linear regressions.

Results T2 measurements were achieved in all cases, and DWI was available in 37 cases. Measurements and ratios were reproducible in eight localizations (i.e. intra- and interobserver ICCs >0.5): frontal T2/thalamus, parietal T2/thalamus, occipital T2/pons, parietal ADC/thalamus, occipital ADC/pons, temporal ADC/pons, occipital ADC and temporal ADC. The frontal T2/thalamus and parietal T2/thalamus correlated with gestational age (P<0.0001 and P=0.014, respectively). In the multivariate modeling, frontal T2/thalamus remained an independent predictor of the gestational age (P<0.0001).

Conclusion The frontal T2/thalamus ratio emerged as a potential additional biomarker of fetal brain maturation during the last trimester of pregnancy.

Keywords Diffusion-weighted magnetic resonance imaging · Fetal brain development · Fetus · Magnetic resonance imaging · T2-weighted magnetic resonance imaging · White matter

Introduction

The detection of white matter abnormalities during the third trimester of pregnancy is challenging in clinical practice because it relies on qualitative and subjective assessment [1, 2]. Fetal white matter physiologically appears with low signal intensity on T1-weighted imaging (WI) and high signal intensity on T2-WI due to its high-water content and incomplete myelination [3, 4]. Hence, pathological high signal intensities on T2-WI can be underdiagnosed. Yet, cerebral white matter abnormalities are not rare among children [5] and may be a sign of a severe brain disorder. Several etiologies can be intertwined such as vascular diseases leading to hypoxic-ischemic damages, infectious diseases, congenital diseases, genetic disorders or metabolic diseases [6–9]. Therefore, objective criteria for assessing fetal white matter abnormalities over time — namely reproducibility, reliability and quantification — are needed, together with other brain biomarkers, in order to improve the prediction of cerebral prognosis.

✉ Jean-François Chateil
jean-francois.chateil@chu-bordeaux.fr

[1] Department of Pediatric Radiology, Pellegrin Hospital, CHU Bordeaux, Place Amélie Raba-Léon, Bordeaux, France

[2] Department of Diagnostic and Interventional Oncologic Imaging, Institut Bergonié, Bordeaux, France

[3] Université de Bordeaux, Bordeaux, France

[4] Centre de Résonance Magnétique des Systèmes Biologiques, UMR 5536, Centre National de la Recherche Scientifique, Université de Bordeaux, F-33076 Bordeaux, France

Previous studies have shown that diffusion-weighted imaging (DWI) with calculation of the apparent diffusion coefficient (ADC) could help date maturation-dependent changes in cerebral white matter and detect diffuse white matter abnormalities [10–16]. However, comparing the results of these studies highlights contrasting conclusions, and when investigated, the inter- and intra-observer agreements of the ADC-based measurements vary for the same region across studies. It should also be noted that no clear consensual methods for measurements have emerged; diverse methods have been used in the literature such as ADC values or ratios. Lastly, DWI is characterized by lower signal-to-noise ratio, lower spatial resolution and being more prone to distortions compared with conventional magnetic resonance imaging (MRI), which may bias its measurements during fetal brain MRI [10].

Furthermore, although T2 sequences provide an excellent contrast for white matter and are constantly acquired in fetal brain protocol, only a few studies have investigated their value in characterizing fetal white matter quantitatively [17–19]. However, the authors did not include the temporal lobe and only one hemisphere per region was assessed. Three studies quantitatively assessed the signal intensities of white matter on T2-WI, but they were based on children and preterm newborns [20–22]. The main drawback of conventional T2-WI is its lack of standardized units, which leads to variability in the interpretation of MRI and makes the use of standardization methods mandatory.

Therefore, we hypothesized that T2-based measurements could improve the estimation of normal white matter maturation in fetuses during the third semester of pregnancy in addition to DWI. To do so, we first defined simple methods to standardize signal intensities and we evaluated their inter- and intra-observer reproducibility. Then we focused on the reproducible T2- and ADC-based measurements to establish the abacus of normative values and to explore univariate and multivariate relationships with gestational age.

Materials and methods

Study design

This retrospective single-center study was approved by our institutional review board. The conditions required in terms of the right to privacy and the protection of health personal data were approved by the data protection officer and the study was recorded in the processing register. As such, the design of the study complies with the general data protection regulation and the framework set by article 65–2 of the French Data Protection Act 2018 as amended, and for clarification does not require any declaration to the supervisory authority. An informational letter with a return form was sent to all patients who satisfied the inclusion criteria. They could indicate their refusal either by e-mail or by mailing back the form. Approval was considered acquired after a month. The patients retained the right to withdraw from the study at any time. Parents who refused the use of their fetal images were excluded.

The records of pregnant women from Jan. 1, 2009, to Oct. 31, 2019, were retrieved from the radiologic database. Fetal MRI indications for patients enrolled in the study were any abnormal outcome in previous pregnancies in siblings or family history (referred to as "family history" in the study), suspected intracranial abnormality or inconclusive findings at fetal ultrasonography, extra-cerebral malformations and suspected mother-to-child infection.

The inclusion criteria were acquisition of a fetal brain MRI at the third trimester of pregnancy at our university hospital, singleton or bichorial-biamniotic twin pregnancy, no abnormal fetal MRI findings, and no brain or neurological abnormality detected prenatally or during postnatal follow-up.

We excluded mothers younger than 18 years old at the time of mail contact, monochorial twin pregnancies, any brain pathology diagnosed by MRI, medical pregnancy termination, poor MRI quality notably due to motion artifacts, mother-to-child infection confirmed by polymerase chain reaction technique in the amniotic fluid retrieved by amniocentesis or in urine at birth, all genetic diseases or chromosomal abnormalities confirmed by karyotype or molecular analysis performed on amniotic fluid, children with an abnormal psychomotor development or any brain pathology diagnosed after birth, and newborns who died during the neonatal period. Moderate and severe ventriculomegalies were excluded because cerebrospinal fluid diapedesis could change the signal intensities in the brain parenchyma. The flowchart for the study is presented in Fig. 1.

The children's psychomotor and cognitive development was assessed by a phone questionnaire (Online Supplementary Material 1) intended to guarantee the inclusion criteria; the children's pediatricians were contacted whenever this was necessary. The development was considered normal if no major psychomotor or cognitive developmental disorder was noticed by the parents or the pediatrician.

The first day of pregnancy and gestational age were established according to the first-trimester ultrasound (US) examination (measure of crown-rump length) between 11 and 13 gestational weeks of amenorrhea + 6 days. Gestational age was expressed in gestational weeks of amenorrhea.

Patients' and children's personal data were pseudonymized and health information was protected.

MRI acquisition

All MRI examinations were performed on a 1.5-tesla (T) magnet (MAGNETOM Avanto VB 19; Siemens Healthineers,

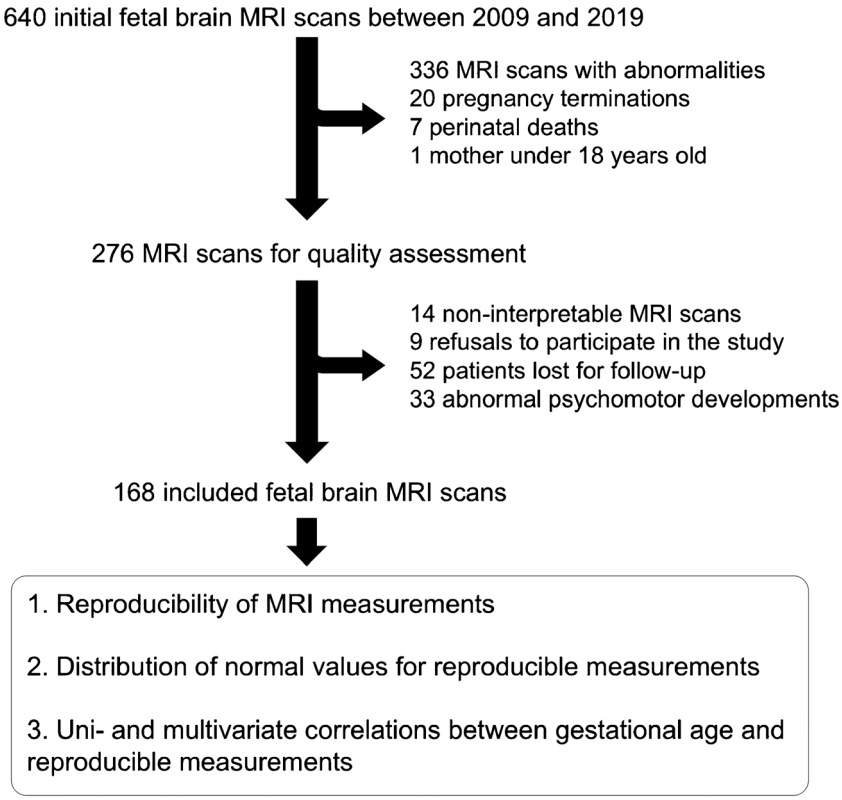

Fig. 1 A flowchart of the study

Erlangen, Germany). Patients were positioned supine with legs slightly raised for comfort or in the left-lateral position.

First, localizers were acquired in axial, sagittal and coronal planes to determine the fetal presentation. A conventional phased array surface body coil was placed over the fetal head; its position over the pelvis could vary slightly depending on the fetal presentation.

The T2-weighted sequence was acquired with a half-Fourier single-shot fast spin echo (HASTE), which provides a good signal-to-noise ratio with an excellent T2-weighted contrast resolution of fetal tissues. The DWI sequence consisted of three orthogonal directions with two b-values (0 and 800 s/mm^2). The ADC maps were automatically generated by using the Siemens Syngovia software. The ADC values were calculated at each voxel according to the mono-exponential equation

$$SI = SI_0 \times \exp.[-b \times ADC]$$

where SI is signal intensity and SI_0 corresponds to the signal intensity without diffusion weighting. The acquisition parameters of these two sequences are described in Table 1.

The other sequences were spin echo true fast imaging with steady-state free precession (TrueFISP) T2-WI, DIXON volumetric interpolated breath-hold examination (VIBE) T1-WI, and gradient echo T1-WI. These three two-dimensional (2-D) sequences were acquired in two orthogonal planes.

Data were subsequently transferred to our picture archiving and communication system for analysis on a dedicated report workstation (Carestream, Noisy-le-Grand, France).

MRI analysis

The radiologic measurements were performed by one junior radiologist (C.L, with 4.5 years of experience in MRI including 6 months of residency in the women and children imaging department of our university hospital) and one senior radiologist (L.C., who specializes in prenatal imaging, with 7 years of experience in fetal MRI).

The following circular regions of interest (ROIs) were drawn manually on the ADC map and the axial T2-WI following previous publications [14, 15]:

(1) right and left frontal white matter (anterior to the frontal horn of the lateral ventricles, avoiding the ventricular zone, at the level of the basal ganglia),
(2) right and left parietal white matter (posterior to the lateral ventricles),
(3) right and left temporal white matter (anterior part of the temporal lobes),
(4) right and left occipital white matter (inferior part of the occipital lobes),

Table 1 Magnetic resonance imaging protocol

Acquisition parameters	2-D T2 single-shot TSE HASTE	2-D DWI single-shot spin echo planar fat sat
Acquisition planes	3 orthogonal plans	Axial
TR (ms)	1,000	2,900
TE (ms)	219	98
Flip angle	180°	–
Acceleration factor	2 (GRAPPA)	2 (GRAPPA)
FOV (mm)	300×300	280×280
In plane resolution (mm^2)	1.7×1.2	2.2×2.2
Slice thickness (mm)	4	3.5
Gap (mm)	0	0.7
Number of slices	20	18
Acquisition time	20 s	57 s
Number of excitation	1	4
Bandwidth (Hz/pixel)	391	1,302
EPI factor	–	128

2-D two-dimensional, *DWI* diffusion-weighted imaging, *EPI* echo planar imaging, *fat sat* fat saturated, *FOV* field of view, *GRAPPA* generalized autocalibrating partial parallel acquisition, *HASTE* half-Fourier acquisition single-shot turbo spin echo, *TE* echo time, *TR* repetition time, *TSE* turbo spin echo

(5) right and left thalamus (in the middle of each thalamus, avoiding the internal capsule),
(6) cerebrospinal fluid (CSF; wherever it was the most available, avoiding partial volume effect) and
(7) pons (in its center).

The ROIs involving the white matter were always drawn in the deep white matter, avoiding the ventricular zone and the subplate.

Figure 2 shows the positioning of the ROIs. We adapted each ROI to the size of the fetal brain and its anatomy. The ROIs were as large as possible but avoided CSF spaces and gray matter. To ensure that the ROIs were representative, whenever it was possible the standard deviation within all voxels had to be less than 10% of the mean value. Otherwise, the ROI size was progressively decreased until reaching this standard deviation [12]. Hence, we extracted the mean signal intensity on T2-WI signal and mean ADC value. All fetal brain MRIs were analyzed by the junior radiologist, and 35 of the 168 fetal brain MRIs were randomly selected and analyzed by the senior radiologist and, a second time, by the junior radiologist (blinded to each other and to the first reading, with a delay of one month between each reading for the junior radiologist) to assess interobserver reliability.

Because of the lack of standardized units regarding the signal intensities of T2-WI, we calculated ratios to make T2-based measurements comparable across different patients, as follows: for the frontal and parietal ROIs, the signal intensity on T2-WI of the thalamus was used as divisor, and for the temporal and occipital ROIs, the signal intensity on T2-WI of the pons was used as divisor. Pons and thalamus were chosen because apparently constant signal intensities decrease during pregnancy. Indeed, to our knowledge, no prenatal modification of the kinetic signal decrease has been described in the literature for these two regions. We also calculated the ratios between the signal intensities on T2-WI of the frontal, parietal, temporal and occipital ROIs and the CSF ROI. Although ADC values are given in standardized units (herein expressed as $\times 10^{-6}$ mm^2/s), we also calculated these three types of ratios for ADC in the four supratentorial brain regions. Throughout the remainder of the study, the term "measurement" refers to the mean T2 signal intensity and ADC value directly extracted from the ROI and the term "calculation" refers to ratios between the two measurements. A summary of the measurements and calculations is given in Online Supplementary Material 2.

Statistical analysis

Statistical analyses were performed with R (version 3.5.3; R Foundation for Statistical Computing, Vienna, Austria) using the tidyverse, irr and BlandAltmanLeh packages [23]. A *P*-value of less than 0.05 was deemed significant. All tests were two-tailed.

Categorical variables were given as numbers and percentages. Numerical variables were given as mean and standard deviation or median and range as appropriate.

Associations between radiologic measurements and calculations and categorical variables (left or right measurements) were assessed with paired Student's *t*-tests or Mann-Whitney tests, depending on the results of the Shapiro-Wilk normality test. In the absence of statistical difference between the left

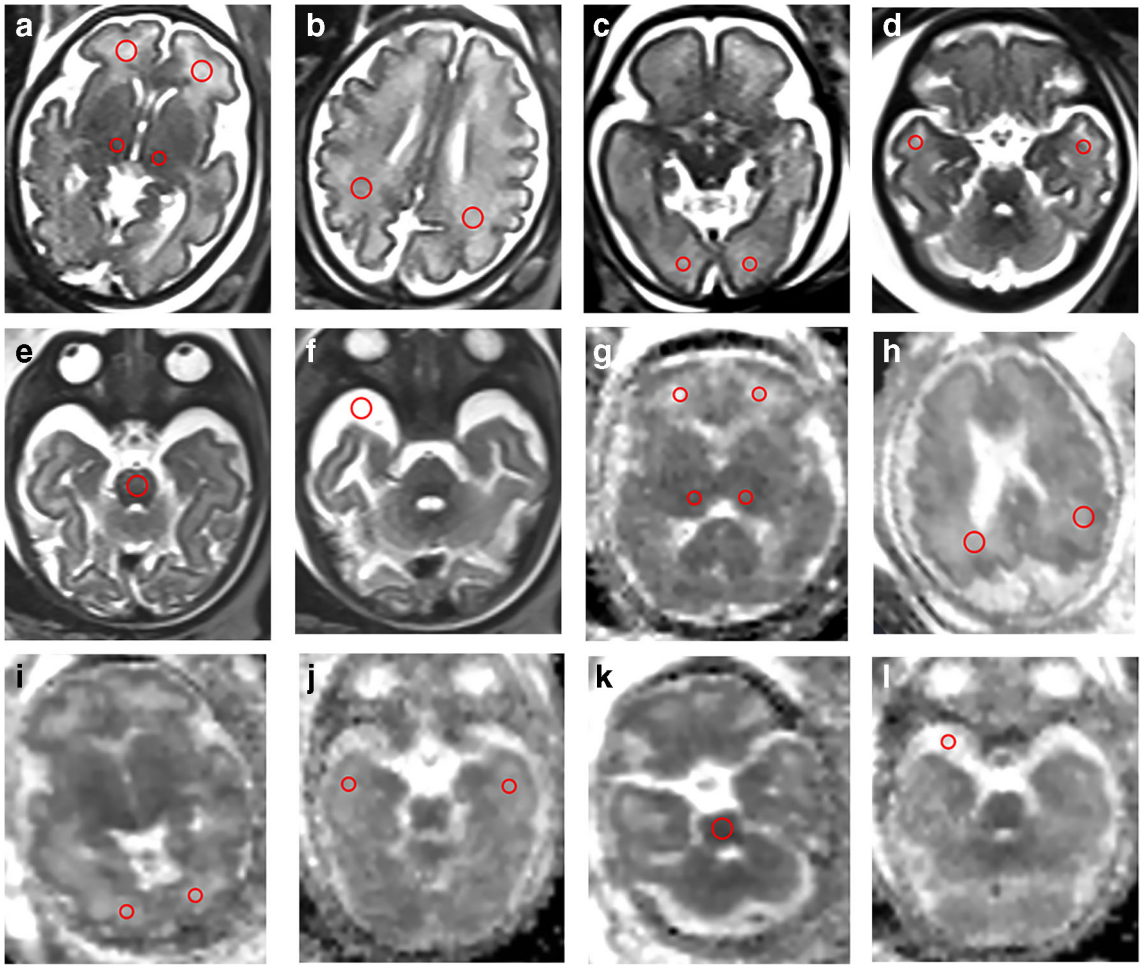

Fig. 2 Positioning of the region of interest in 28–35 weeks gestational age fetuses. **a**–**f** Axial T2-weighted imaging (T2-WI). **g**–**l** Axial apparent diffusion coefficient (ADC) maps from diffusion-weighted imaging. The regions of interest are positioned in the right and left frontal white matter and right and left thalamus (**a** and **g**), the right and left parietal white matter (**b** and **h**), the right and left occipital white matter (**c** and **i**), the right and left temporal white matter (**d** and **j**), the center of the pons (**e** and **k**), and the cerebrospinal fluid (**f** and **l**)

and the right, left and right radiologic measurements and calculations were averaged for the rest of the study.

Inter- and intra-observer agreements were estimated with intraclass correlation coefficients (ICC) using a two-way random effect model determining absolute agreement between the radiologists. An ICC of less than 0.50 indicates poor reliability; consequently only radiologic measurements with inter- and intra-observer ICCs ≥0.50 were selected for building abacus and developing models to estimate fetal brain age. They will be referred to as reproducible measurements or calculations in the rest of the manuscript. Correlations between these reproducible radiologic measurements and calculations were evaluated with the Spearman rank test.

Inter- and intra-observer Bland-Altman plots were built for each reproducible measurement and calculation by plotting the mean absolute difference (or bias) and its limits of agreements (defined as mean of the bias ± 1.96 × standard deviation) as a function of the average of the measurement of the two readings.

Next, we evaluated the distribution and summary statistics of each reproducible measurement and calculation by estimating its median, range, mean, standard deviation and 95% confidence interval (CI) at each week of the third trimester of pregnancy.

To build a simple model to estimate the fetal brain age (i.e. gestational age for a healthy pregnancy), we first assessed correlations between each reproducible radiologic measurement and calculation and the gestational age with univariate linear regressions. Second, all the reproducible measurements and calculations with a *P*-value of less than 0.2 at univariate analysis were entered into a multivariate linear regression model. The modeling performances were estimated with the coefficient of determination (or adjusted R^2), which corresponds to the proportion of the variance in the variable to predict, explained by the explanatory variables of interest in the model and adjusted for the number of these explanatory variables.

Results

Study population

In total, 168 unique fetal brain MRIs were included. Table 2 summarizes the study population. Gestational age ranged from 28 to 37 weeks. The median age of the mothers during fetal brain MRI was 30 years (range: 16–47 years). The median follow-up after childbirth (i.e. child age) was 5 years (range: 0.7–11 years). There were nine bichorial-biamniotic twin pregnancies. The main indication for a fetal MRI was a suspicion of fetal brain pathology at ultrasonography in 100/168 (59.5%) patients followed by family history (29/168, 17.3%) and a suspicion of other organ malformations during ultrasono-graphy (27/168, 16.1%). The most frequent benign findings on MRI were a mild ventriculomegaly (27/168, 16.1%) and subependymal pseudocysts facing the frontal horns (24/168, 14.3%).

Table 2 Characteristics of the study population (numbers of patients with percentage in parentheses except for ages)

Characteristics	Patients
Gestational age range (weeks)	28–37
Child age at clinical evaluation (years)	
Mean (SD)	4.9±3.1
Median (range)	4.7 (0.7–11)
Maternal age at time of MRI (years)	
Mean (SD)	30.0±5.6
Median (range)	30 (16–47)
Child gender	
Boy	86/168 (51.2%)
Girl	82/168 (48.8%)
Indication for fetal brain MRI	
Suspected brain pathology at US	100/168 (59.5%)
Family history	29/168 (17.3%)
Suspected other organs malformation at US	27/168 (16.1%)
Intrauterine growth restriction	4/168 (2.4%)
Hydramnios	3/168 (1.8%)
Suspected congenital cytomegalovirus infection	3/168 (1.8%)
Alloimmunization (HLA, platelet)	2/168 (1.2%)
Twin malformation in a bichorial-biamniotic pregnancy	2/168 (1.2%)
Drug intake	1/168 (0.6%)
Maternal subarachnoid hemorrhage	1/168 (0.6%)
Suspected fetal brain pathology at US	
Mild ventriculomegaly (between 10 and 12 mm)	29/100 (29%)
Frontal subependymal pseudocysts	24/100 (24%)
Cerebral biometry inferior to the 5th percentile	15/100 (15%)
Abnormality of cavum septum pellucidum	11/100 (11%)
Suspected abnormality of corpus callosum	8/100 (8%)
Abnormality of posterior fossa	6/100 (6%)
Choroid plexus cyst	3/100 (3%)
Cerebral biometry superior to the 90th percentile	3/100 (3%)
Small suprasellar cyst	2/100 (2%)
Enlarged pericerebral spaces	1/100 (1%)
Enlarged 3rd ventricle	1/100 (1%)
Fetal brain MRI findings	
Mild ventriculomegaly (between 10 and 12 mm)	27/168 (16.1%)
Frontal subependymal pseudocysts	24/168 (14.3%)
Cerebral biometry at the lower limit	5/168 (3%)
Dolichocephaly	5/168 (3%)
Mildly enlarged cisterna magna	4/168 (2.4%)
Cavum vergae	4/168 (2.4%)
Isolated choroid plexus cyst	2/168 (1.2%)
Cerebral biometry at the upper limit	4/168 (2.4%)
Isolated arachnoid cyst	2/168 (1.2%)
3rd ventricle at the upper limit of normal	1/168 (0.6%)
Pericerebral spaces at the upper limit of normal	1/168 (0.6%)
Normal corpus callosum	1/168 (0.6%)

HLA human leucocyte antigen, *MRI* magnetic resonance imaging, *SD* standard deviation, *US* ultrasonography

The sizes of the ROIs depended on the gestational age and the brain region of interest, as follows: the average area was 20 mm^2 in the frontal white matter (range: 13–40 mm^2), 28 mm^2 in the parietal white matter (range: 17–45 mm^2), 18 mm^2 in the temporal white matter (range: 7–30 mm^2), 10 mm^2 in the occipital white matter (range: 5–18 mm^2), 15 mm^2 in the thalamus (range: 8–30 mm^2), 45 mm^2 in the CSF (range: 25–60 mm^2) and 17 mm^2 in the pons (range: 6–25 mm^2).

Comparison of left and right measurements

The comparisons of the measurements and calculations depending on the laterality are in Online Supplementary Material 3. They did not show any statistical difference; consequently, the average of the left and right measurements (or calculations) was used in the whole study.

Reproducibility of measurements

Table 3 shows the inter- and intra-observer agreements for the four brain locations (a visual representation is given in Online Supplementary Material 4). In total, 11 measurements and calculations demonstrated both intra- and interobserver ICCs ≥0.5 when also including T2-based measurements without ratio. T2-based calculations were reproducible for frontal T2/thalamus (ICC_{intra}=0.886, ICC_{inter}=0.791), parietal T2/thalamus (ICC_{intra}=0.803, ICC_{inter}=0.711) and occipital T2/pons (ICC_{intra}=0.736, ICC_{inter}=0.587), but not for temporal T2/pons (ICC_{intra}=0.643, ICC_{inter}=0.031). Finally, eight measurements and calculations were selected for the rest of the study: frontal T2/thalamus, parietal T2/thalamus, parietal ADC/thalamus, occipital T2/pons, occipital ADC/pons, occipital ADC, temporal ADC/pons and temporal ADC.

Bland-Altman plots for these eight measurements and calculations are given in Fig. 3. No visual relationship was observed between their mean and their absolute difference (bias and limits of agreements for each plot are given in Online Supplementary Material 5). Regarding ratios, the largest inter- and intra-observer biases were found with occipital ADC/pons (0.077, limits of agreements: −0.18–0.333) and temporal ADC/pons (0.074, limits of agreements: −0.188–0.335), respectively. Both largest inter- and intra-observer limits of agreements were found with occipital T2/pons (−0.044, limits of agreements: −0.654–0.566 and 0.001, −0.393–0.396, respectively).

Table 3 Inter- and intra-observer intraclass correlation coefficients for each measurement and calculation

Indices	Intra-observer agreement		Interobserver agreement	
	ICC (95% CI)	*P*-value	ICC (95% CI)	*P*-value
Frontal T2/thalamus	0.886 (0.787–0.940)	<0.0001	0.791 (0.623–0.889)	<0.0001
Parietal T2/thalamus	0.803 (0.644–0.896)	<0.0001	0.711 (0.497–0.843)	<0.0001
Temporal T2/pons	0.643 (0.403–0.802)	<0.0001	0.031 (−0.294–0.353)	0.43
Occipital T2/pons	0.736 (0.535–0.858)	<0.0001	0.587 (0.321–0.767)	0.0001
Frontal T2/CSF	0.488 (0.189–0.704)	0.0011	0.331 (0.017–0.591)	0.019
Parietal T2/CSF	0.197 (−0.141–0.494)	0.13	0.340 (0.010–0.603)	0.022
Temporal T2/CSF	0.573 (0.305–0.758)	0.0001	0.104 (−0.233–0.418)	0.27
Occipital T2/CSF	0.509 (0.225–0.716)	0.0005	0.474 (0.167–0.696)	0.002
Frontal ADC/thalamus	0.795 (0.459–0.933)	0.0002	0.496 (−0.091–0.825)	0.045
Parietal ADC/thalamus	0.841 (0.570–0.948)	0.0001	0.575 (0.002–0.858)	0.025
Temporal ADC/pons	0.519 (0.031–0.818)	0.019	0.542 (0.009–0.840)	0.023
Occipital ADC/pons	0.795 (0.473–0.932)	0.0002	0.597 (0.099–0.862)	0.011
Frontal ADC/CSF	0.888 (0.683–0.964)	<0.0001	−0.285 (−0.694–0.304)	0.84
Parietal ADC/CSF	0.801 (0.460–0.935)	0.0004	−0.045 (−0.565–0.515)	0.56
Temporal ADC/CSF	0.699 (0.252–0.898)	0.0035	−0.182 (−0.632–0.397)	0.74
Occipital ADC/CSF	0.563 (0.039–0.843)	0.019	0.004 (−0.443–0.520)	0.49
Frontal T2	0.938 (0.882–0.968)	<0.0001	0.904 (0.818–0.950)	<0.0001
Parietal T2	0.951 (0.905–0.975)	<0.0001	0.926 (0.860–0.962)	<0.0001
Temporal T2	0.909 (0.828–0.953)	<0.0001	0.320 (0.001–0.584)	0.025
Occipital T2	0.931 (0.861–0.965)	<0.0001	0.901 (0.814–0.949)	<0.0001
Frontal ADC	0.877 (0.649–0.960)	<0.0001	0.328 (−0.207–0.736)	0.11
Parietal ADC	0.817 (0.503–0.940)	0.0002	0.212 (−0.357–0.679)	0.23
Temporal ADC	0.651 (0.178–0.879)	0.0063	0.525 (−0.038–0.835)	0.032
Occipital ADC	0.841 (0.568–0.948)	0.0001	0.633 (0.139–0.877)	0.0078
Thalamus T2	0.959 (0.920–0.979)	<0.0001	0.960 (0.924–0.980)	<0.0001
Thalamus ADC	0.806 (0.441–0.938)	0.0005	0.200 (−0.320–0.662)	0.23
Pons T2	0.912 (0.832–0.955)	<0.0001	0.932 (0.869–0.965)	<0.0001
Pons ADC	0.737 (0.307–0.913)	0.0017	0.815 (0.476–0.943)	0.0004
CSF T2	0.883 (0.780–0.939)	<0.0001	0.826 (0.684–0.908)	<0.0001
CSF ADC	0.845 (0.669–0.950)	<0.0001	−0.106 (−0.663–0.488)	0.63

ADC apparent diffusion coefficient, *CI* confidence interval, *CSF* cerebrospinal fluid, *ICC* intraclass correlation coefficient

Regarding ADC values, the largest inter- and intra-observer biases were found with occipital ADC (0.07, limits of agreements: −0.156–0.295 and −0.016, limits of agreements: −0.173–0.14, respectively). The largest inter- and intra-observer limits of agreements were found with temporal ADC (0.029, limits of agreements: −0.229–0.288) and occipital ADC (−0.016, limits of agreements: −0.173–0.14).

Distribution of the reproducible measurements and calculations

Figure 4 represents the mean values (with 95% CI when estimable) of the eight reproducible measurements at each week of the third semester (the numerical details are shown in Online Supplementary Material 6). In particular, frontal T2/thalamus progressively and constantly increased with gestational age. Regarding ADC-related measures, it should be noted that only 2/29 (7.1%) measures were available at 28 weeks, 1/29 (3.6%) at 29 weeks and none at 30, 36 and 37 weeks. Hence, the 95% CIs were not estimated at these time points.

Correlations between reproducible measurements and calculations

The correlation matrix of the eight reproducible measurements can be found in Online Supplementary Material 7. The three most significant positive correlations were found between temporal ADC and occipital ADC (rho=0.62, *P*=0.0002),

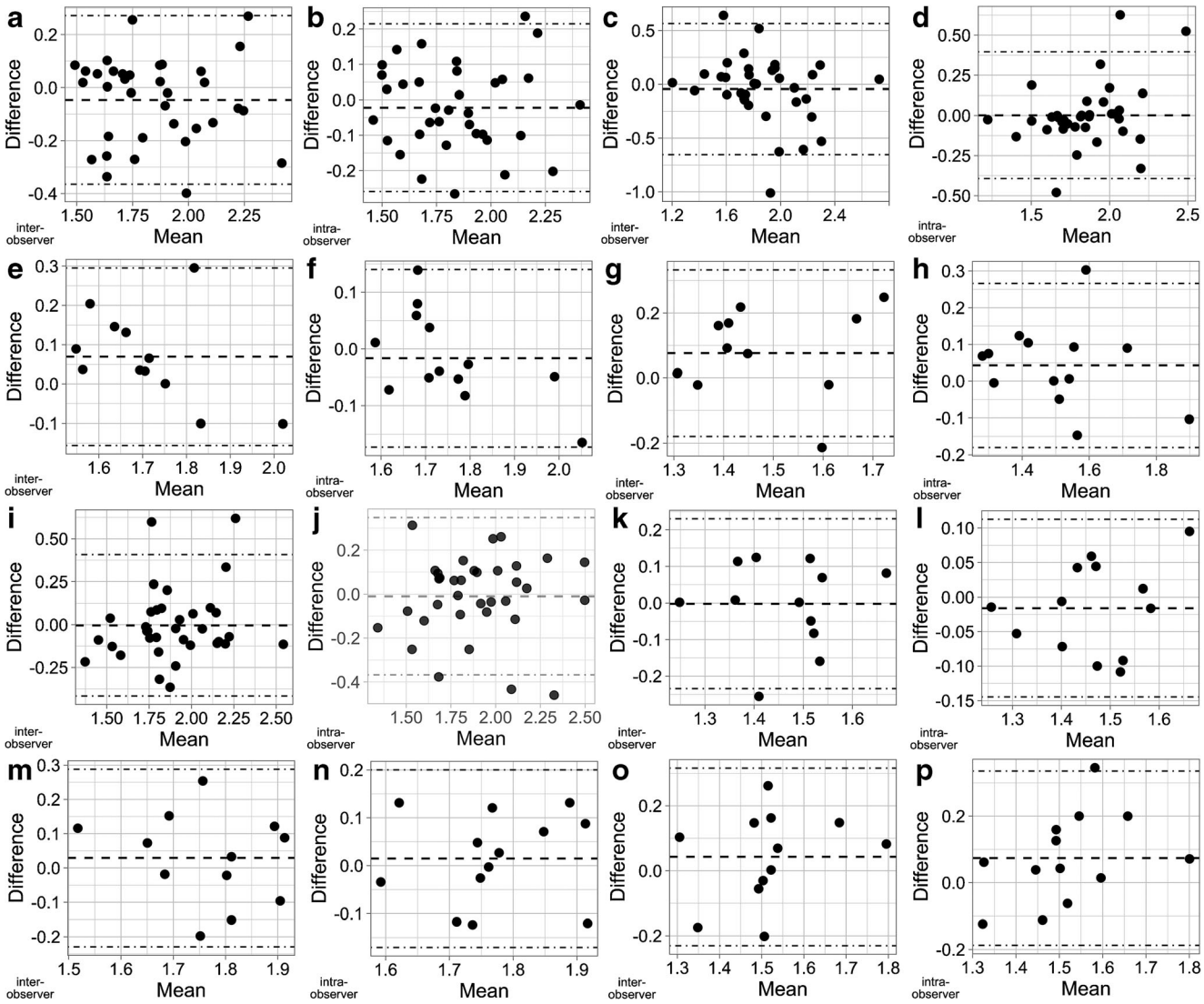

Fig. 3 Interobserver (**a, c, e, g, i, k, m, o**) and intra-observer (**b, d, f, h, j, l, n, p**) Bland-Altman plots for the eight reproducible measurements and calculations: frontal T2/thalamus (**a, b**), occipital T2/pons (**c, d**), occipital apparent diffusion coefficient (ADC) (**e, f**), occipital ADC/pons (**g, h**), parietal T2/thalamus (**i, j**), parietal ADC/thalamus (**k, l**), temporal ADC (**m, n**) and temporal ADC/pons (**o, p**). *T2* T2-weighted sequence

temporal ADC/pons and occipital ADC/pons (rho=0.61, P<0.0001) and occipital ADC/pons and occipital T2/pons (rho=0.45, P=0.0030). None of the negative correlations reached significance.

Univariate and multivariate correlations between reproducible measurements and calculations and gestational age

Table 4 shows the results of the univariate linear regression modeling between gestational age and the reproducible measurements. Three of them reached significance. There was a positive linear relationship between gestational age and frontal T2/thalamus (adjusted R^2=0.194 and P<0.0001, Fig. 7) and between gestational age and parietal T2/thalamus (adjusted R^2=0.030, P=0.014, Fig. 5). A significant negative relationship was initially found between gestational age and occipital ADC (adjusted R^2=0.115, P=0.043). However, a careful analysis of the scatterplot reveals an extreme observation (upper left of the graph at a gestational age of 29 weeks) that was responsible for the significance. Removal of this outlier led to insignificant correlation (P=0.49); therefore, occipital ADC was not included in the multivariate analysis (Fig. 6). Removing two possible outliers for parietal T2/thalamus strengthened the result and, consequently, we kept these observations in the subsequent modeling. When the frontal T2/thalamus and parietal T2/thalamus variables were entered in a multivariable linear regression model, frontal T2/thalamus remained independently correlated with gestational age (P<0.0001) but not parietal T2/thalamus (P=0.37) (Table 5).

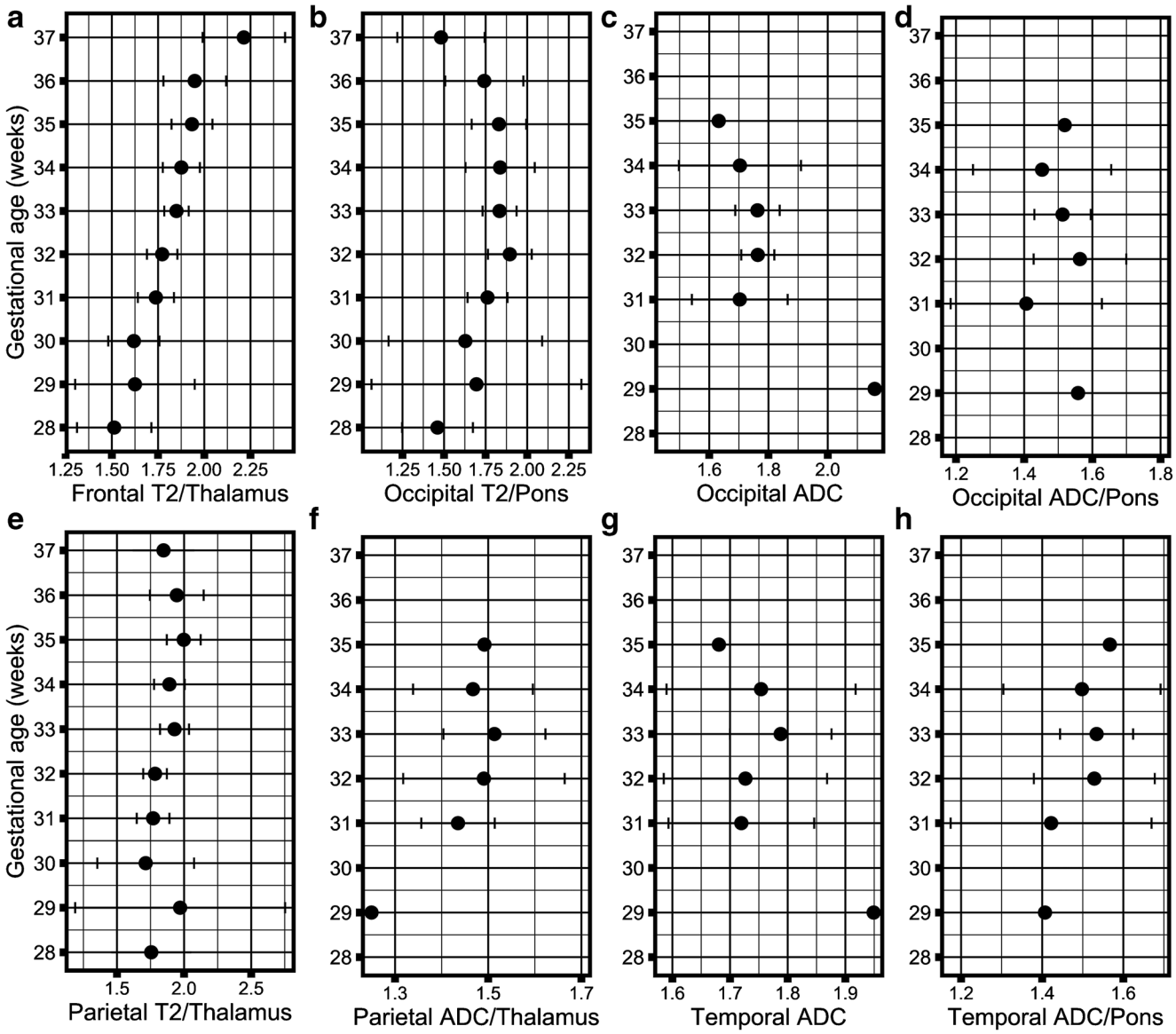

Fig. 4 Distribution of reproducible measurements. **a** Frontal T2/thalamus. **b** Occipital T2/pons. **c** Occipital apparent diffusion coefficient (ADC). **d** Occipital ADC/pons. **e** Parietal T2/thalamus. **f** Parietal ADC/thalamus. **g** Temporal ADC. **h** Temporal ADC/pons

Discussion

Establishing objective and quantifiable criteria of normal MRI white matter signal intensity according to gestational age is a critical prerequisite to diagnosing signal intensity abnormalities. Our aim was to investigate the contribution of quantitative T2-based variables and DWI to establish objective criteria of normal white matter signal intensity during the last trimester of pregnancy. The assessment of inter- and intra-observer reproducibility between operators is a crucial step in each biomarker study. After checking for the comparability of left and right values, we filtered the T2- and DWI-based measurements and calculations according to their ICCs before investigating their potential correlation with the gestational age. We found that 8 of the 20 measurements and calculations were reproducible (without considering the non-standardized T2 measurements in each lobe): frontal T2/thalamus, parietal T2/thalamus, occipital ADC, occipital ADC/pons, occipital T2/pons, parietal ADC/thalamus, temporal ADC/pons and temporal ADC.

There is a lack of consensus on the best technique for harmonizing signal intensities in MRI data sets. Several techniques for intensity harmonization have been proposed in the neuroimaging literature to enable robust analysis of structural and diffusion MRIs across different radiologic centers and longitudinally [24–28]. However, these techniques require an advanced post-processing tool and are too time-consuming to be used in clinical practice. Herein, we propose

Table 4 Univariate linear regressions between reproducible measurements, calculations and gestational age

Indices	Slope	Constant term	Adjusted R^2	*P*-value
Frontal T2/thalamus	3.472	26.534	0.194	<0.0001
Parietal T2/thalamus	1.182	30.671	0.030	0.014
Parietal T2/thalamus *without outliers*	*1.524*	*30.068*	*0.052*	*0.0018*
Parietal ADC/thalamus	2.523	29.028	0.019	0.22
Temporal ADC		35.249	−0.020	0.50
Temporal ADC/pons	1.908	29.878	0.005	0.30
Occipital T2/pons	0.392	32.180	−0.0005	0.34
Occipital ADC	−3.486	38.831	0.115	0.043
Occipital ADC *without outlier*	*−1.270*	*35.084*	*−0.020*	*0.49*
Occipital ADC/pons	−0.263	33.144	−0.038	0.89

The linear relationship can be expressed as gestational age = slope × (measurement or calculation) + constant term. In the equation, ADC is expressed as $\times 10^{-3}$ mm^2/s. Ratios of two measurements do not have units. Results are given with and after the removal of outliers identified in the graphic representations of the relationships (Figs. 5 and 6) and, in the latter case, are indicated in italics. *ADC* apparent diffusion coefficient, *T2* T2-weighted sequence

a simpler method to harmonize the different MRIs, using ratios with a specific brain region as a signal intensity reference [12, 19, 24, 29, 30]. We chose three distinct references to calculate ratios and to standardize T2 and ADC values in the four brain regions. However, we found that none of the ratios with CSF was reproducible, and we were not able to investigate a possible influence of the MRI system with this method because all the MRI examinations were performed on the same system. It should be noted that our ROIs were smaller than those in previous studies [11–16, 31, 32]. Although using small ROIs enabled us to reduce the partial volume effect with the adjacent CSF, ventricular cavity and cortex, it might have resulted in a subsampling of voxels. Conversely, even though we drew ROIs of small dimensions, it was sometimes difficult to place them while respecting all the criteria detailed in the methods, especially in the temporal lobes and at the end of the third trimester because of the gyration progression. Therefore, we cannot formally exclude that small parts of ventricular zone or subplate were accidentally measured. The slice thickness also can influence the values of these measurements and

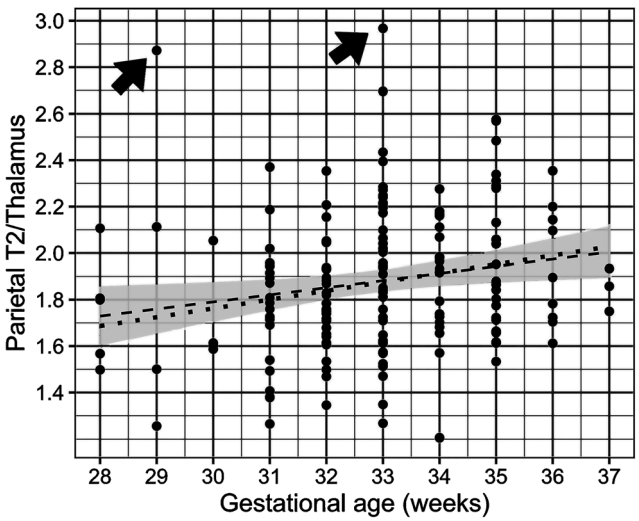

Fig. 5 Assessment of univariate linear relationship between gestational age and parietal T2/thalamus ratio. The shaded area represents the 95% confidence interval. Two regression lines were drawn. The first (*dashed line*) included all the observations and can be expressed as gestational age=30.671+1.182×parietal T2/thalamus ratio (*P*=0.014). The second (*dotted line*) was drawn after removing two extreme values at 29 weeks and 33 weeks (*arrows*) and can be expressed as gestational age=30.068+1.524×parietal T2/thalamus ratio (*P*=0.0018)

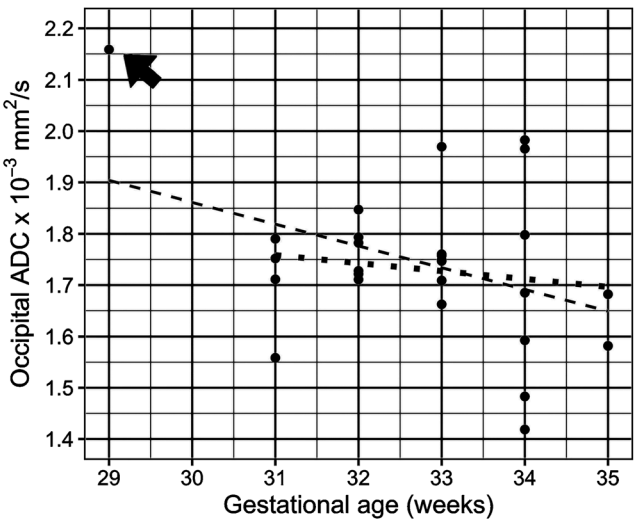

Fig. 6 Assessment of linear relationship between gestational age and occipital apparent diffusion coefficient (ADC). Two regression lines were drawn. The first (*dashed line*) included all observations and can be expressed as gestational age=28.831−3.486×occipital ADC (*P*=0.043). The second (*dotted line*) was drawn after removing an extreme value at 29 weeks (*arrow*) and can be expressed as gestational age=35.084+1.270×occipital ADC (*P*=0.49)

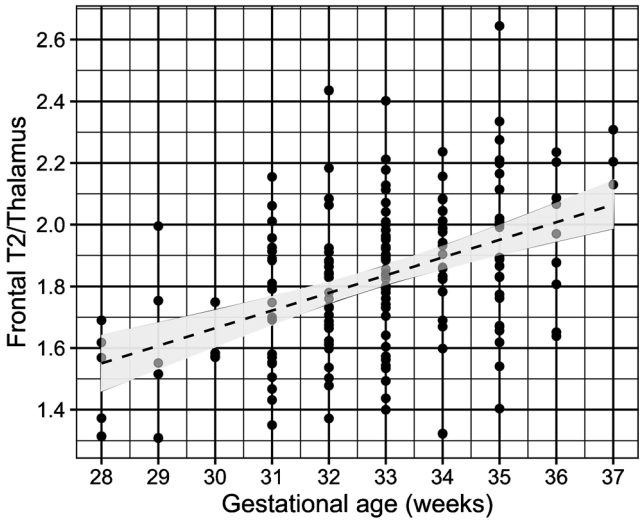

Fig. 7 Assessment of linear relationship between gestational age and frontal T2/thalamus ratio. The shaded area represents the 95% confidence interval. The regression line (*dashed line*) can be expressed as gestational age=26.534+3.472×frontal T2/thalamus ratio (P<0.0001)

calculations. Herein, the thickness of T2-WI and DWI were standardized and in range with other studies.

We chose the CSF signal intensity as a divisor because its composition is considered stable during pregnancy [29, 33, 34]. The poor reproducibility for CSF and CSF-related calculations can be explained by the lack of standard ROI positioning in the CSF. Indeed, we placed these ROIs wherever CSF was more abundant to avoid partial volume effect. Regarding the poor reproducibility of the temporal T2/pons ratio, we hypothesize that it was due to a lower surface of white matter available for measurement compared to the other lobes and also to a higher risk of partial volume effect. Thus, this positioning could change from one fetus to another. In the study by Leroy et al. [29], the signal intensity references (namely the vitreous body and CSF) were measured on the ipsilateral side of the structure of interest [19]. That way, the different variables were similarly affected by the low-frequency spatial variations of the signal due to radio frequency inhomogeneities [24, 29]. However, this study did not assess intra- and interobserver reproducibility.

Previous studies have shown that DWI and ADC can help detect diffuse white matter abnormalities, which have been shown to correlate with autism, mental retardation, hypotonia, ataxia, spasticity or neurosensorial impairments, for instance [6]. Yet, these studies, as well as our study, highlighted contrasting conclusions [10–16]. Indeed, while some authors found that ADC was relatively stable between 26 and 33 gestational weeks, others demonstrated significant positive or negative relationships with gestational age depending on the brain regions.

In agreement with previous studies, we found a tendency toward a negative correlation between the gestational age and the occipital ADC values, although the result did not reach significance after the outlier analysis [12, 13, 35, 36]. This relationship may be related to a decrease in brain water content and an increase in the concentration of macromolecules such as myelin and lipids [13, 37, 38].

Interestingly, we found that the two reproducible measurements from DWI were ADC values without ratios. This finding suggests that ADC does not require additional standardization since it is already given in standardized units. In addition, we highlighted significant and positive correlations between temporal ADC and occipital ADC, between temporal ADC/pons and occipital ADC/pons, and between occipital ADC/pons and occipital T2/pons. These results suggest similarities in the development of white matter in brain temporal and occipital region during the third trimester of pregnancy, in terms of cellularity, neuronal maturation and myelination. Further studies would be needed to investigate this point.

Reproducibility was lacking for the frontal and parietal ADC values and hardly reached statistical significance for the temporal ADC. This may be due to the relatively small number of fetuses with DWI in our series because this sequence has recently been implemented in our routine fetal MRI protocol.

In this study, we have shown that frontal T2/thalamus signal intensity ratio is a reproducible calculation, which is significantly and positively correlated with the gestational age in univariate as well as in multivariate analyses. Additionally, this correlation was independent in multivariate modeling.

The significant positive correlation found between gestational age and frontal T2/thalamus and parietal T2/thalamus can be explained by a faster and earlier decrease in signal for the thalami compared to the frontal and parietal lobes. These

Table 5 Results of multivariate linear regression modeling

Term	Coefficient	Standard error	P-value	Model adjusted R^2
Frontal T2/thalamus	3.317	0.569	<0.0001	0.192
Parietal T2/thalamus	0.405	0.454	0.37	
Constant term	26.058	1.144	–	

The relationship between gestational age (GA) and MRI measurements can be expressed as GA ≈ 3.317 × frontal T2/thalamus + 0.454 × parietal T2/thalamus + 26.058

findings have been described by Abe et al. [19] and Cannie et al. [16]. Indeed, myelination proceeded from central to peripheral and posterior to anterior, with a beginning of myelination seen on T2 around a gestational age of 24–25 weeks for thalami and between 1 and 2 years of life for the frontal lobe [37, 39, 40]. Additionally, the maturation of astrocytes and neurons within the thalami may also contribute to a decrease in free water content and therefore a reduction in T2 values [21]. The temporal distribution of the myelination process could explain why a significant relationship with gestational age was not found for our other reproducible measurements and calculations. Indeed, since myelination appears complete on T2 by the age of 2 years old we cannot exclude the possibility of interindividual variability regarding the myelination during the third trimester of gestation. Assessing myelination over a longer period, beyond birth, and in larger cohorts may smooth this variability.

It should be noted that interobserver agreement was not reproducible for temporal T2/pons, which is an important fact considering that in congenital cytomegalovirus infections, white matter hyperintensities are frequently observed in temporal lobe.

After multivariate modeling, we found that only frontal T2/thalamus was correlated with gestational age. Hence, our retrospective exploratory study strongly suggests that frontal T2/thalamus could improve the estimation of the gestational age. However, with an adjusted R^2 of less than 0.200, this measurement alone would be insufficient to predict the real gestational age from new data. We believe predictive models could be improved by including other MRI measurements from MR spectroscopy, diffusion tensor imaging or quantitative assessment of the gyration patterns through shape analysis [41]. However, functional MRI techniques are difficult to use in clinical practice because of motion-induced artifacts, poor signal-to-noise ratio and relatively long scan time.

Our study has limitations. First, only 37 MRIs included DWI because this sequence has only been recently included in our routine MRI protocol, whereas it has been performed for a long time and in a consistent manner in other centers. Since most DWI sequences were performed on fetuses between 30 and 35 weeks, the multivariate model combining DWI and T2 measurements could not be used below and above these gestational ages. The lack of data below 30 weeks of gestational age can be explained by French legislation; medical pregnancy termination is possible until term in France, which is not the case in most countries [42]. Thus, fetal brain MRIs are preferably performed from 32 weeks of gestational age to improve the spatial resolution and to better qualify the gyration. Furthermore, the children did not have a medical evaluation during the follow-up, but a phone questionnaire by a non-specialized physician. Optimally, the postnatal evaluation should have been done by a pediatrician with the help of a standardized scale, such as the Brunet-Lezine Révisée scale [43]. Moreover, we included fetuses with intrauterine growth restriction due to a vascular cause as long as they displayed normal brain biometry, no neurodevelopmental adverse outcome and a normal weight curve by the time of the phone contact. In addition, we did not investigate if alternative ROI positionings could have strengthened the relationship between MRI measurements/ratios and the fetal brain age. Finally, our method for segmenting the brain areas (namely 2-D ROIs on normally appearing lobar white matter) can be questioned in pathological situations (either focal or diffuse diseases) because ROIs are at risk of sampling bias. Future studies should investigate if using automated extraction of lobar white matter through deep learning algorithms followed by a deeper quantification of structural patterns through radiomic textural analysis could more accurately identify abnormal maturation of the fetal brain.

Conclusion

This study identified an original reproducible measurement, the frontal T2/thalamus ratio, which strongly correlated with gestational age in univariate and multivariate modeling. Therefore, frontal T2/thalamus could be a valuable adjunct to diffusion-based measurements in order to estimate the maturation of the fetal brain during the last trimester of pregnancy. Future independent and, ideally, prospective cohorts in healthy and pathological conditions, including biological correlates, should confirm if frontal T2/thalamus ratio could be used as a surrogate biomarker to improve the assessment of fetal brain maturation during the last trimester of pregnancy in addition to diffusion-weighted imaging.

Supplementary Information The online version contains supplementary material available at https://doi.org/10.1007/s00247-021-05064-1.

Acknowledgements We thank Dr. Catherine Garel for her thorough review and her thoughtful remarks during the writing of this article.

Declarations

Conflicts of interest None

References

1. Diogo MC, Glatter S, Binder J et al (2020) The MRI spectrum of congenital cytomegalovirus infection. Prenat Diagn 40:110–124
2. Lipitz S, Hoffmann C, Feldman B et al (2010) Value of prenatal ultrasound and magnetic resonance imaging in assessment of congenital primary cytomegalovirus infection. Ultrasound Obstet Gynecol 36:709–717
3. Garel C (2004) The role of MRI in the evaluation of the fetal brain with an emphasis on biometry, gyration and parenchyma. Pediatr Radiol 34:694–699
4. Averill LW, Kandula VVR, Akyol Y, Epelman M (2015) Fetal brain magnetic resonance imaging findings in congenital

cytomegalovirus infection with postnatal imaging correlation. Semin Ultrasound CT MR 36:476–486
5. Dangouloff-Ros V, Roux C-J, Boulouis G et al (2019) Incidental brain MRI findings in children: a systematic review and meta-analysis. AJNR Am J Neuroradiol 40:1818–1823
6. Kristjnsdóttir R, Uvebrant P, Wiklund LM (2000) Clinical characteristics of children with cerebral white matter abnormalities. Eur J Paediatr Neurol 4:17–26
7. Fazekas F, Kleinert R, Offenbacher H et al (1993) Pathologic correlates of incidental MRI white matter signal hyperintensities. Neurology 43:1683–1689
8. Katorza E, Strauss G, Cohen R et al (2018) Apparent diffusion coefficient levels and neurodevelopmental outcome in fetuses with brain MR imaging white matter hyperintense signal. AJNR Am J Neuroradiol 39:1926–1931
9. Neuberger I, Garcia J, Meyers ML et al (2018) Imaging of congenital central nervous system infections. Pediatr Radiol 48:513–523
10. Garel C (2006) New advances in fetal MR neuroimaging. Pediatr Radiol 36:621–625
11. Hoffmann C, Weisz B, Lipitz S et al (2014) Regional apparent diffusion coefficient values in 3rd trimester fetal brain. Neuroradiology 56:561–567
12. Sartor A, Arthurs O, Alberti C et al (2014) Apparent diffusion coefficient measurements of the fetal brain during the third trimester of pregnancy: how reliable are they in clinical practice? Prenat Diagn 34:357–366
13. Schneider JF, Confort-Gouny S, Le Fur Y et al (2007) Diffusion-weighted imaging in normal fetal brain maturation. Eur Radiol 17: 2422–2429
14. Boyer AC, Gonçalves LF, Lee W et al (2013) Magnetic resonance diffusion-weighted imaging: reproducibility of regional apparent diffusion coefficients for the normal fetal brain. Ultrasound Obstet Gynecol 41:190–197
15. Schneider MM, Berman JI, Baumer FM et al (2009) Normative apparent diffusion coefficient values in the developing fetal brain. AJNR Am J Neuroradiol 30:1799–1803
16. Cannie M, De Keyzer F, Meersschaert J et al (2007) A diffusion-weighted template for gestational age-related apparent diffusion coefficient values in the developing fetal brain. Ultrasound Obstet Gynecol 30:318–324
17. Stazzone MM, Hubbard AM, Bilaniuk LT et al (2000) Ultrafast MR imaging of the normal posterior fossa in fetuses. AJR Am J Roentgenol 175:835–839
18. Huisman TAGM, Martin E, Kubik-Huch R, Marincek B (2002) Fetal magnetic resonance imaging of the brain: technical considerations and normal brain development. Eur Radiol 12:1941–1951
19. Abe S, Takagi K, Yamamoto T et al (2004) Semiquantitative assessment of myelination using magnetic resonance imaging in normal fetal brains. Prenat Diagn 24:352–357
20. Leppert IR, Almli CR, McKinstry RC et al (2009) T(2) relaxometry of normal pediatric brain development. J Magn Reson Imaging 29: 258–267
21. Counsell SJ, Kennea NL, Herlihy AH et al (2003) T2 relaxation values in the developing preterm brain. AJNR Am J Neuroradiol 24:1654–1660
22. Thornton JS, Amess PN, Penrice J et al (1999) Cerebral tissue water spin-spin relaxation times in human neonates at 2.4 tesla: methodology and the effects of maturation. Magn Reson Imaging 17: 1289–1295
23. Wickham H, Averick M, Bryan J et al (2019) Welcome to the Tidyverse. J Open Source Softw 4:1686
24. Vovk U, Pernus F, Likar B A review of methods for correction of intensity inhomogeneity in MRI. IEEE Trans Med Imaging 26: 405–421
25. Sun X, Shi L, Luo Y et al (2015) Histogram-based normalization technique on human brain magnetic resonance images from different acquisitions. Biomed Eng Online 14:73
26. Fortin J-P, Sweeney EM, Muschelli J et al (2016) Removing inter-subject technical variability in magnetic resonance imaging studies. Neuroimage 132:198–212
27. De Nunzio G, Cataldo R, Carlà A (2015) Robust intensity standardization in brain magnetic resonance images. J Digit Imaging 28: 727–737
28. Yu M, Linn KA, Cook PA et al (2018) Statistical harmonization corrects site effects in functional connectivity measurements from multi-site fMRI data. Hum Brain Mapp 39:4213–4227
29. Leroy F, Glasel H, Dubois J et al (2011) Early maturation of the linguistic dorsal pathway in human infants. J Neurosci 31:1500–1506
30. Glasser MF, Van Essen DC (2011) Mapping human cortical areas in vivo based on myelin content as revealed by T1- and T2-weighted MRI. J Neurosci 31:11597–11616
31. Bui T, Daire J-L, Chalard F et al (2006) Microstructural development of human brain assessed in utero by diffusion tensor imaging. Pediatr Radiol 36:1133–1140
32. Righini A, Bianchini E, Parazzini C et al (2003) Apparent diffusion coefficient determination in normal fetal brain: a prenatal MR imaging study. AJNR Am J Neuroradiol 24:799–804
33. Autti T, Raininko R, Vanhanen SL et al (1994) MRI of the normal brain from early childhood to middle age. I. Appearances on T2- and proton density-weighted images and occurrence of incidental high-signal foci. Neuroradiology 36:644–648
34. Luoma K, Raininko R, Nummi P, Luukkonen R (1993) Is the signal intensity of cerebrospinal fluid constant? Intensity measurements with high and low field magnetic resonance imagers. Magn Reson Imaging 11:549–555
35. Cartry C, Viallon V, Hornoy P, Adamsbaum C (2010) Diffusion-weighted MR imaging of the normal fetal brain: marker of fetal brain maturation. J Radiol 91(5 Pt 1):561–566
36. Han R, Huang L, Sun Z et al (2015) Assessment of apparent diffusion coefficient of normal fetal brain development from gestational age week 24 up to term age: a preliminary study. Fetal Diagn Ther 37:102–107
37. Barkovich AJ, Kjos BO, Jackson DE, Norman D (1988) Normal maturation of the neonatal and infant brain: MR imaging at 1.5 T. Radiology 166:173–180
38. Baumann N, Pham-Dinh D (2001) Biology of oligodendrocyte and myelin in the mammalian central nervous system. Physiol Rev 81: 871–927
39. Gao W, Lin W, Chen Y et al (2009) Temporal and spatial development of axonal maturation and myelination of white matter in the developing brain. AJNR Am J Neuroradiol 30:290–296
40. Hasegawa M, Houdou S, Mito T et al (1992) Development of myelination in the human fetal and infant cerebrum: a myelin basic protein immunohistochemical study. Brain Dev 14:1–6
41. Garel C, Chantrel E, Elmaleh M et al (2003) Fetal MRI: normal gestational landmarks for cerebral biometry, gyration and myelination. Childs Nerv Syst 19:422–425
42. Cassart M, Garel C (2020) European overview of current practice of fetal imaging by pediatric radiologists: a new task force is launched. Pediatr Radiol 50:1794–1798
43. Brunet O, Lézine I, Josse D (1997) Brunet-Lézine révisé: échelle de développement psychomoteur de la première enfance : manuel BLR-C. Issy-Les-Moulineaux (France): Etablissements d'Applications Psychotechniques